Dependence of the organic nonvolatile memory performance on the location of ultra-thin Ag film

2010 J. Phys. D: Appl. Phys. 43 035101

(http://iopscience.iop.org/0022-3727/43/3/035101)

IOP PUBLISHING JOURNAL OF PHYSICS D: APPLIED PHYSICS

J. Phys. D: Appl. Phys. **43** (2010) 035101 (7pp) doi:10.1088/0022-3727/43/3/035101

Dependence of the organic nonvolatile memory performance on the location of ultra-thin Ag film

Bo Jiao[1], Zhaoxin Wu[1,3], Qiang He[1], Yuan Tian[2], Guilin Mao[1] and Xun Hou[1]

[1] Key Laboratory for Physical Electronics and Devices of the Ministry of Education, School of Electronic and Information Engineering, Xi'an Jiaotong University, Xi'an, Shaanxi, 710049, People's Republic of China

[2] Department of Electronic Science and Technology, School of Electronic and Information Engineering, Xi'an Jiaotong University, Xi'an, Shaanxi, 710049, People's Republic of China

E-mail: zhaoxinwu@mail.xjtu.edu.cn

Received 23 July 2009, in final form 14 October 2009
Published 8 January 2010
Online at stacks.iop.org/JPhysD/43/035101

Abstract

We demonstrated organic nonvolatile memory devices based on 4,4′,4″-*tris*[*N*-(3-methylphenyl)-*N*-phenylamino] triphenylamine (*m*-MTDATA) inserted by an ultra-thin Ag film. The memory devices with different locations of ultra-thin Ag film in *m*-MTDATA were investigated, and it was found that the location of the Ag film could affect the performance of the organic memory, such as ON/OFF ratio, retention time and cycling endurance. When the Ag film was located at the ITO/*m*-MTDATA interface, the largest ON/OFF ratio (about 10^5) could be achieved, but the cycling endurance was poor. When the Ag film was located in the middle region of the *m*-MTDATA layer, the ON/OFF ratios came down by about 10^3, but better performance of cycling endurance was exhibited. When the Ag film was located close to the Al electrode, the ON/OFF ratios and the retention time of this device decreased sharply and the bistable phenomenon almost disappeared. Our works show a simple approach to improve the performance of organic memory by adjusting the location of the metal film.

(Some figures in this article are in colour only in the electronic version)

1. Introduction

Organic nonvolatile memories are accepted as next-generation data-storage devices because of their simple device structure, low fabrication cost and large variation of organic chemical structure [1, 2]. Several configurations have been developed for organic memory, such as organic/metal/organic devices [3, 4], ITO/metal/organic devices [5], organic bilayer devices [6], polymer or small-molecule MIM devices [7–9], metal-organic composite devices [10] and organic-based donor–acceptor devices [11]. Among these structures of organic memory devices, devices with organic/metal/organic and ITO/metal/organic structures can achieve better memory performance, and devices with these two structures have been extensively demonstrated, such as 2-amino-4,5-imidazole dicarbonitrile/Al/2-amino-4,5-imidazole dicarbonitrile [3, 4], polyfluorene/Ag/polyfluorene [12], *N*,*N*′-biphenyl-*N*,*N*′-bis(1-naphthyl)-(1, 1′-biphenyl)-4,4′-diamine/Al/*N*,*N*′-biphenyl-*N*,*N*′-*bis*(1-naphthyl)-(1, 1′-biphenyl)-4,4′-diamine [13], *tris*-(8-hydroxyquinoline) aluminium/Al (Mg, Ag, Cr)/*tris*-(8-hydroxyquinoline) aluminium [13, 14] and ITO/Ag/poly(*N*-vinylcarbazole) [5]. However, the influence of locations of the metal layer in organic layer on the memory performance has not been investigated systematically.

In this work, organic nonvolatile memories with an organic/metal/organic structure using 4,4′, 4″-*tris*[*N*-(3-methylphenyl)-*N*-phenylamino]triphenylamine(*m*-MTDATA) (figure 1(*a*)) inserted by an ultra-thin Ag film with the thickness of 0.5 nm are demonstrated, and we have investigated the

[3] Author to whom any correspondence should be addressed.

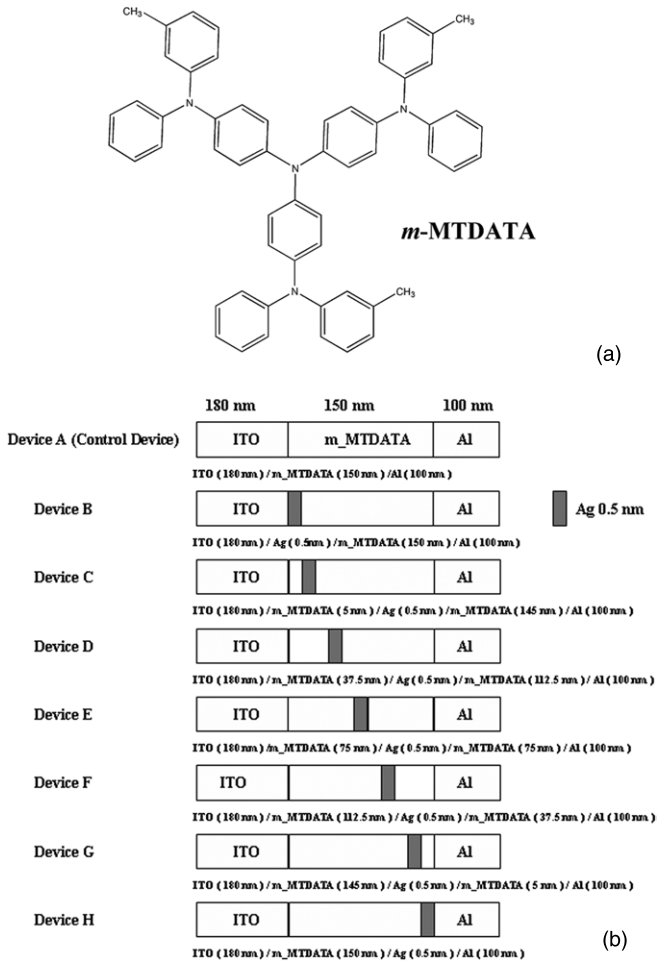

Figure 1. Molecular structures of *m*-MTDATA (*a*) and the configurations of devices A–H in the experiment (*b*). Al is used as anode and ITO as cathode here.

dependence of the organic memory performance on locations of the ultra-thin Ag film in the *m*-MTDATA layer. It is found that the efficiency of organic memory, such as on/off ratio, data retention ability and cycling endurance, was strongly affected by the Ag film location. This could be a simple approach to improve the performance of organic memory by adjusting the location of the metal film.

2. Experiments

In our experiments, the organic memory devices were built on glass substrates precoated with an indium tin oxide (ITO) film with a thickness of 180 nm. The pressure during thermal evaporation for deposition was about 5×10^{-4} Pa. *m*-MTDATA, Ag and Al were deposited at the rates of 0.3 nm s^{-1}, 0.01 nm s^{-1} and 0.2 nm s^{-1}, respectively, without vacuum break. Al was used as the anode and ITO as the cathode. The thickness of the films was determined *in situ* by a quartz-crystal sensor and *ex situ* by a profilometer. The area of the devices was 12 mm^2 for all the samples studied in this work. The current–voltage (I–V) curves, the retention time under stress conditions and the cycling endurance characteristics of the devices were measured by a computer-controlled sourcemeter (Keithley 2602). The surface morphology of the film was characterized by tapping-mode atomic force microscopy (AFM, Nanoscope Dimension 3100, veeco). All the measurements were carried out at room temperature under ambient conditions.

Eight types of devices were fabricated to study the influence of the inserting position to the performance of the organic memory. Their configurations are shown as follows (figure 1(*b*)):

(1) Device A (*control device*): ITO/*m*-MTDATA (150 nm)/Al (100 nm).
(2) Device B: ITO/Ag (0.5 nm)/*m*-MTDATA (150 nm)/Al (100 nm).
(3) Device C: ITO/*m*-MTDATA (5 nm)/Ag (0.5 nm)/*m*-MTDATA (145 nm)/Al (100 nm)
(4) Device D: ITO/*m*-MTDATA (37.5 nm)/Ag (0.5 nm)/*m*-MTDATA (112.5 nm)/Al (100 nm)
(5) Device E: ITO/*m*-MTDATA (75 nm)/Ag (0.5 nm)/*m*-MTDATA (75 nm)/Al (100 nm)
(6) Device F: ITO/*m*-MTDATA (112.5 nm)/Ag (0.5 nm)/*m*-MTDATA (37.5 nm)/Al (100 nm)
(7) Device G: ITO/*m*-MTDATA (145 nm)/Ag (0.5 nm)/*m*-MTDATA (5 nm)/Al (100 nm)
(8) Device H: ITO/*m*-MTDATA (150 nm)/Ag (0.5 nm)/Al (100 nm)

3. Current density–voltage characteristics

Current density–voltage (J–V) characteristics of devices A–H are shown in figures 2(*a*)–(*h*), respectively. For devices B–F, their J–V characteristics were obtained by sweeping the voltage from 15 to −15 V, and then from −15 to 15 V. For devices A, G and H, however, their J–V characteristics were obtained by sweeping the voltage from 15 to −10 V, and then from −10 to 15 V, because their high current densities at −10 V are close to the breakdown current of the devices. Device A without an inserted Ag layer was defined as the control device. As shown in figure 2(*a*), the J–V curves of the control device did not show notable bistable phenomena. When a 0.5 nm thick Ag film was inserted at the ITO/*m*-MTDATA interface, such as device B (figure 2(*b*)), remarkably bistable phenomena with high ON/OFF ratios of 10^5 could be observed in the positive voltage region. Just as shown in figure 2(*b*), as the voltage was swept from 15 to −15 V, the device was in a high-resistance state (OFF state), when the voltage was swept from −15 to 15 V, the device was in a low-resistance state (ON state). While the Ag film was located in the region between the ITO/*m*-MTDATA interface and the middle of the *m*-MTDATA layer, such as devices C–E (figures 2(*c*)–(*e*)), the bistable phenomena are still notable, but the ON/OFF ratios decreased to 10^3. While the Ag film was located in the region between the middle of the *m*-MTDATA layer and the *m*-MTDATA/Al interface, such as devices F and G (figures 2(*f*)–(*g*)), the bistable phenomena were sharply weakened, and the ON/OFF ratios were no larger than 10. When the Ag film was located at the *m*-MTDATA/Al interface, such as device H, the bistable phenomena almost disappeared. The ON/OFF ratios of devices A–H in the sweep J–V characteristics at a readout

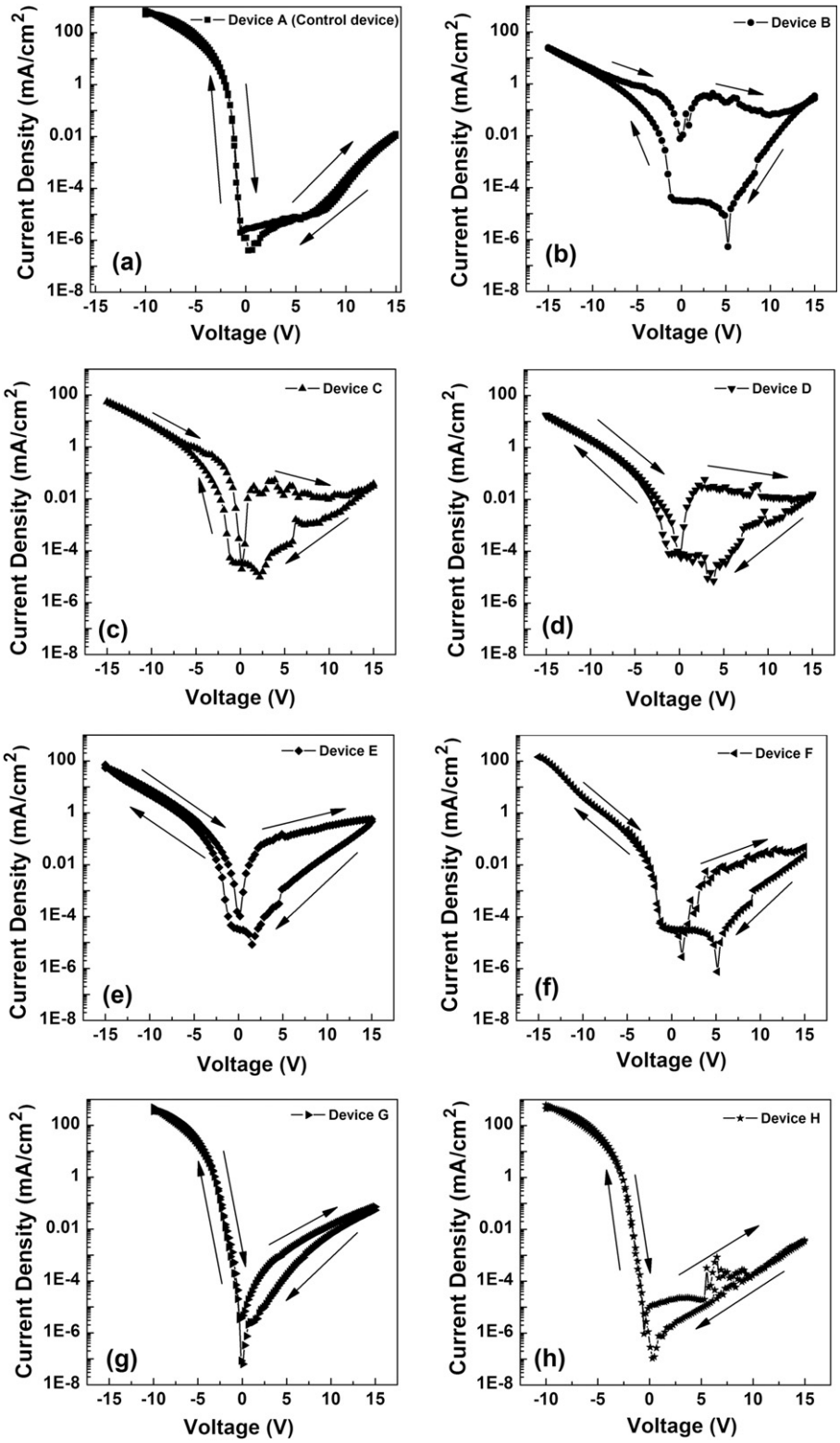

Figure 2. Current density–voltage (J–V) characteristics of devices A–H.

voltage of 3.0 V are summarized in table 1. In the negative bias region, the current density was at the same level as the control device for devices where the Ag film was inserted close to the aluminium electrode, such as devices G and H. For devices where the Ag film was inserted far away from the aluminium electrode, such as devices B–F, however, their current densities in the reverse bias region were sharply decreased compared with that of the control device.

It was also found that the bistable phenomena of devices B–F strongly depended on the initial voltage of the sweep from the reverse direction. Taking device E as an example (figure 3), when the initial voltage of the sweep was less

Table 1. Summary of ON/OFF ratios at readout voltage of 3.0 V and threshold voltages (V_{th}) for devices A–G.

Devices	ON/OFF	V_{th} (V)
Device A[a]	NA	NA
Device B	10^2–10^5	−11
Device C	10^2–10^3	−11 to −12
Device D	10^2–10^3	−11 to −12
Device E	10^2–10^3	−11
Device F	10	−10 to −11
Device H[a]	Less than 10	−10
Device G[a]	NA	NA

[a] The largest initial voltages of devices A, H and G are all −10 V. When initial voltage larger than −10 V is applied, those devices always break down.

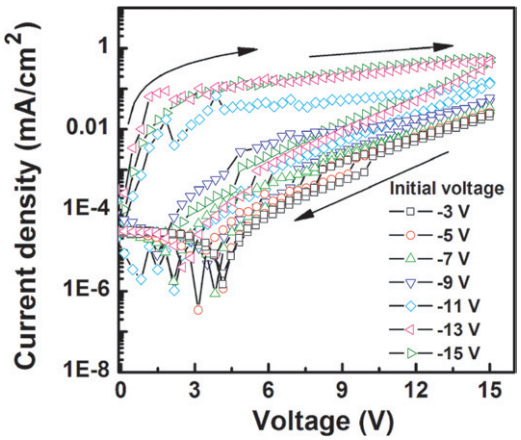

Figure 3. Current–voltage characteristics of device E. Al and ITO are used as anode and cathode, respectively. The legend indicates the initial voltage of the sweep.

than −9 V, no obvious bistable phenomena could be observed. When the initial voltage reached −9 V, low ON/OFF ratio bistable phenomena appeared. As the initial voltage increased to −11 V, larger ON/OFF ratio bistable phenomena could be observed. Then, with the increase in the initial voltage, the ON state current density and the OFF current density almost increased with the same proportion at the same readout voltage, and the ON/OFF ratio was in the same level of that of the sweep from −11 V. The minimum initial voltage that could induce the largest ON/OFF ratio bistable phenomena was defined as the threshold voltage (V_{th}), which is different from the definition of Bozano *et al* [14]. In their report, V_{th} indicates the voltage at which a device initially in the OFF state increases its conductance. The V_{th} of devices A–G is summarized in table 1. As shown in table 1, V_{th} values of devices B–H are all around −11 V, indicating that the V_{th} is independent of the location of the ultra-thin Ag film.

A possible explanation for the bistable phenomena is the charge traps caused by the deposition of the ultra-thin Ag film [14]. In previous reports, it has been demonstrated that unreactive metallic atoms, such as Ag atom, will diffuse into the bulk of the organic films when they are deposited onto the organic film during the initial phase of film formation [15, 16]. Hence, the 0.5 nm thick Ag layer in our devices is too thin to be a uniform film and it exists in the forms of diffused atoms as well as islands. The AFM images of the surface of the 0.5 nm thick Ag layer deposited on the m-MTDATA film are shown as additional evidence in figure 4. Figure 4(a) shows the AFM image of the surface of m-MTDATA film with a thickness of 75 nm. Figure 4(*b*) shows the AFM image of the surface of the 0.5 nm thick layer of Ag deposited on the m-MTDATA film with a thickness of 75 nm. The root-mean-square (RMS) of surface roughness of the 75 nm thick m-MTDATA film is 0.401 nm, while that of the 0.5 nm thick Ag layer is 0.597 nm. Figure 4(*b*) indicates the formation of the separated Ag small islands. Height image of the 0.5 nm thick Ag layer is shown in figure 4(*c*), which indicates that the diameters of the separated Ag small islands vary from 10 to 50 nm. Because of the wide-band-gap property of m-MTDATA, the highest occupied molecular orbital and the lowest unoccupied molecular orbital which are of −5.1 eV and −1.9 eV, respectively [17], the diffused Ag atoms and these islands will form deep impurity levels in the m-MTDATA material, which form the charge traps, just as shown in figure 5. When the device is biased at a sufficient initial reverse voltage which is higher than the V_{th} (see figure 5(*a*), ITO and Al are used as the anode and as the cathode, respectively), deep impurity levels will be filled with holes injected from ITO and a space-charge field will build up, which will cause a band bending. While the bias is swept to a positive voltage, hole injection is restrained by the large barrier between the Fermi energy of Al (−4.3 eV) and the HOMO level of m-MTDATA (−5.1 eV). However, the electron injection from ITO is enhanced due to the band bending, which makes the device in the ON state (see figure 5(*b*), ITO and Al are used as the cathode and as the anode, respectively). With the increase in the positive bias, the injected electrons combine with the trapped holes and the space-charge field gradually disappears. Hence, the current is decreased and a negative differential resistance region is formed. While the bias is swept back to zero, electron injection is restrained by the great offset between the Fermi energy of ITO (−4.5 eV) and the LUMO level of m-MTDATA (−1.9 eV), and hole injection is restrained by the great offset between the Fermi energy of Al and the HOMO level of m-MTDATA. Thus, the current will be kept in the OFF state. The effect of charge trapping by silver was also demonstrated in the report of Ma *et al*, where the Ag trapping levels were formed by the diffusion of Ag atoms during the evaporation of Ag electrode on the organic layer [9].

As shown in figures 2(*b*)–(*h*) and table 1, ON/OFF ratios of memory devices obviously depend on the location of the Ag film in devices. According to the above discussions, we can conclude that the charge trapping effects of the deep impurity levels of Ag were influenced by the locations of itself in the devices. In our devices, the Al electrode was fabricated by evaporating aluminium onto the *m*-MDTATA layer, which will induce diffusion of aluminium atoms into the *m*-MDTATA layer. Many techniques, such as angle resolved XPS (ARXPS) [18] and medium energy ion scattering (MEIS) [19] spectroscopy, have been used to study the diffused behaviour of aluminium atoms during the evaporation of Al electrode onto the organic film. It has been reported that the concentration of diffused aluminium atoms in the organic layer decreased dramatically along the depth direction. For instance,

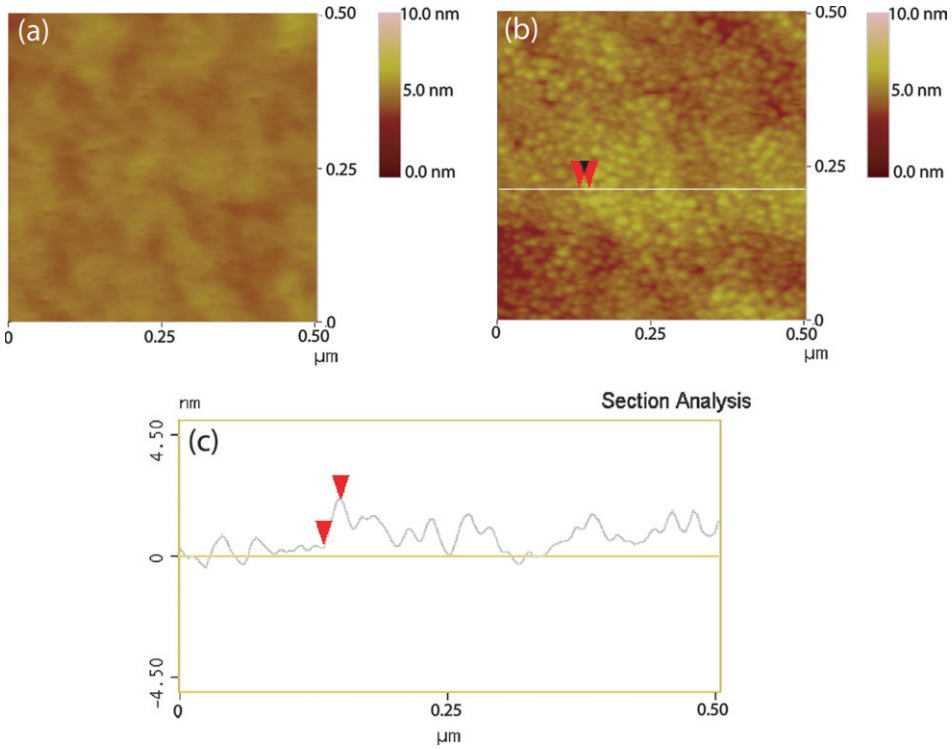

Figure 4. Tapping-mode AFM images of surface of the 75 nm thick *m*-MTDATA film (*a*) (RMS = 0.401 nm) and of the 0.5 nm thick Ag layer (*b*) deposited on the 75 nm thick *m*-MTDATA film (RMS = 0.597 nm). Height image of the 0.5 nm thick Ag layer along the line section in figure 1(*b*) is also shown (*c*). Silicon wafer was chosen as substrate for these two samples. (Scan size: 0.5 × 0.5 μm).

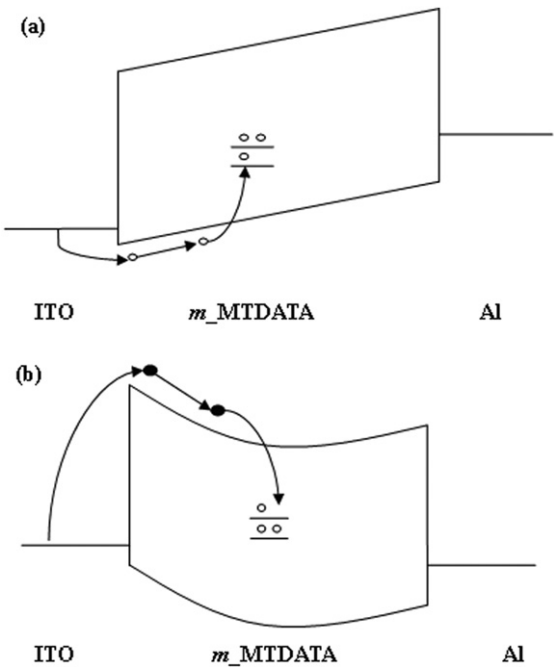

Figure 5. Schematic energy level structures of organic NDR device in the experiment at reverse biases (ITO and Al are used as anode and cathode, respectively) (*a*) and forward biases (Al and ITO are used as anode and cathode, respectively) (*b*).

the concentration of diffused aluminium at the position of 10 nm away from the Al/organic interface is less than a quarter of that near the Al/organic interface [18, 19]. Therefore, for devices where the ultra-thin Ag layer is inserted close to the Al/*m*-MTDATA interface (see figure 6(*a*)), such as devices G and H, the diffused aluminium atoms around the Ag layer will affect the charge trapping effect of deep impurity levels of Ag atoms. For instance, figure 6(*a*) shows the possibility of the formation for conductive filament between the Ag atoms and Al electrode increased [20], which can accelerate the escape of trapped charges. As a result, the ON/OFF ratio of those devices sharply decreased. However, for devices where the ultra-thin Ag layer is inserted far away from the Al/*m*-MTDATA interface (see figure 6(*b*)), such as devices B–F, no diffused aluminium atoms influence the charge trapping effect of Ag atoms. Thus, the dependence of ON/OFF ratios on the location of the Ag film can be attributed to the influence of diffusion behaviour of aluminium atoms in the bulk of the *m*-MTDATA layer.

4. Data retention and cycling endurance

Data retention tests under stress conditions for devices B–F were carried out with a readout voltage of 3 V. The readout currents of devices B–F as a function of time are shown in figure 7. Just as shown in figure 7, for all devices except device F, the current density almost does not change with time over 1000 s. For device F, however, the current density dramatically decreases with time, and data retention time of device F is no more than 100 s.

The cycling endurance performances of devices B–F were investigated by applying 1000 sequential WRITE–READ–ERASE–READ voltage pulses. Voltages for WRITE, ERASE and READ were −15 V, 15 V and 3 V, respectively. Devices C, D, E and F all show good cycling endurance larger than

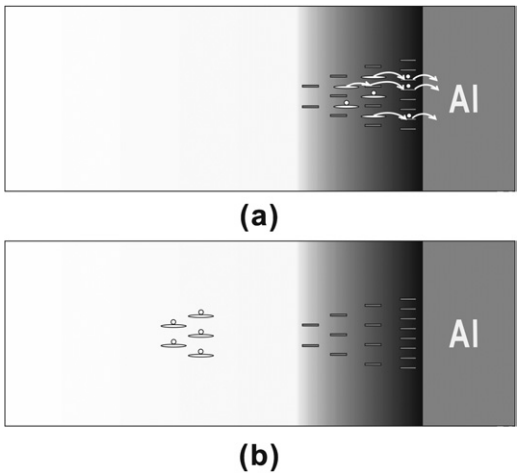

Figure 6. Schematic structures of the devices where the ultra-thin Ag layer is inserted close to the Al/*m*-MTDATA interface, such as devices G and H (*a*), and the devices where the ultra-thin Ag layer is inserted far away from the Al/*m*-MTDATA interface, such as devices B–F (*b*).

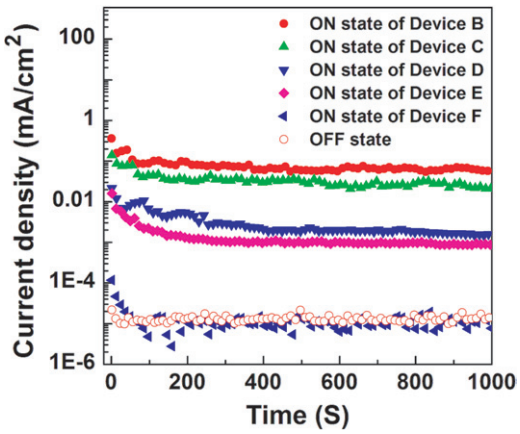

Figure 7. Data retention tests under stress conditions for devices B–F. The OFF state current densities of the five devices are all around the same level, so one OFF state line is chosen as a representative.

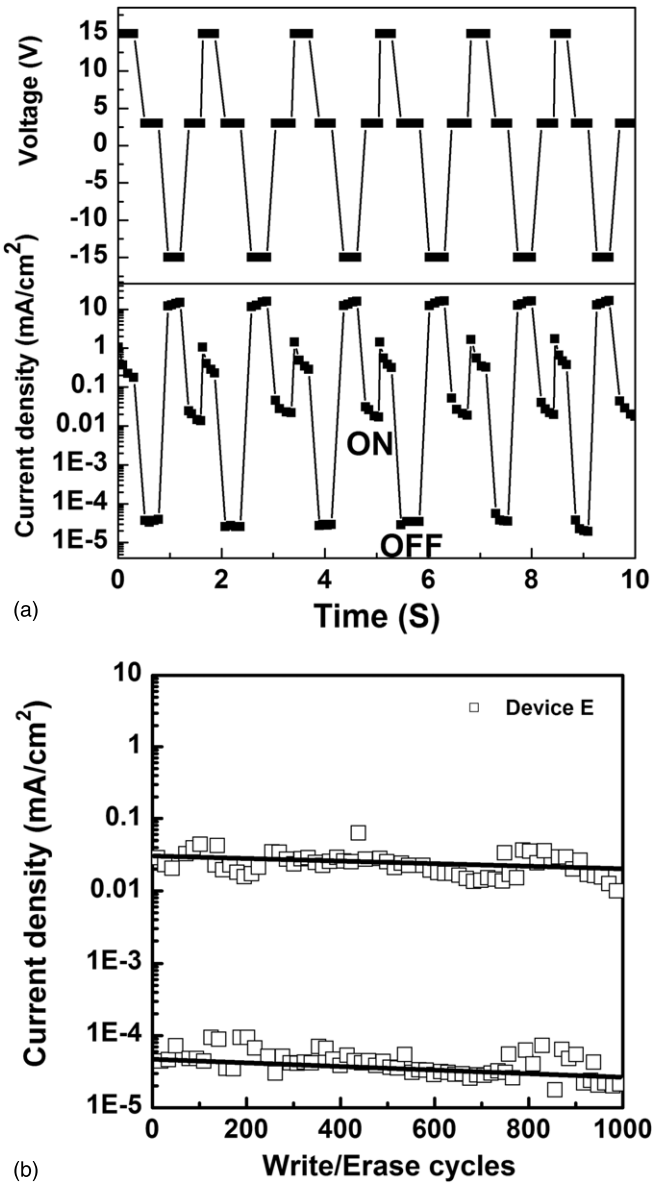

Figure 8. Applied voltage sequence, E(15 V)–R(3 V)–W(-15 V)–R(3 V), and the current density responses (*a*) and 1000 cycles on–off test result (*b*) for device E, respectively. The line is a guide to the eye.

1000 cycles. Just as shown in figure 8(*a*), taking device E as a representative, the current density response of the memory device followed the applied cyclic voltage sweep very well. The difference between two alternate READ currents demonstrates the ON and OFF states of the bit stored in the memory device. As shown in figure 8(*b*), during the 1000 cycles test process, device E exhibited good reliability and rewritability with ON/OFF ratios around 10^3, which exhibits the potential in the field of memory and switching applications. In contrast, device B exhibited poor reliability performance during the cycling test process, and the ON/OFF ratios were reduced thousand times after 600 cycles, just as shown in figure 9. Recently, Kondo *et al* have reported a stable, high ON/OFF ratio organic memory device using ITO surfaces modified by Ag-nanodots [5]. In their work, a bridging reagent, 4-mercaptobenzoic acid, was used to enhance the adhesion force between Ag-NPs and ITO surface and the memory device showed good cycling endurance. So the poor stability of device B in our experiments may result from the weak interaction between Ag atoms and ITO surfaces, and the physical details are still under further study.

5. Conclusion

Organic/metal/organic type memory devices based on *m*-MTDATA inserted by an ultra-thin Ag film have been investigated. By comparing the performance of the memory devices with different locations of the ultra-thin Ag film, we have found that the performance of the organic memory, such as ON/OFF ratio, retention time and cycling endurance, strongly depends on the location of the ultra-thin Ag layer. For devices where the Ag film was located in the ITO/*m*-MTDATA interface, largest ON/OFF ratio but poor cycling endurance could be achieved. However, for devices where the Ag film

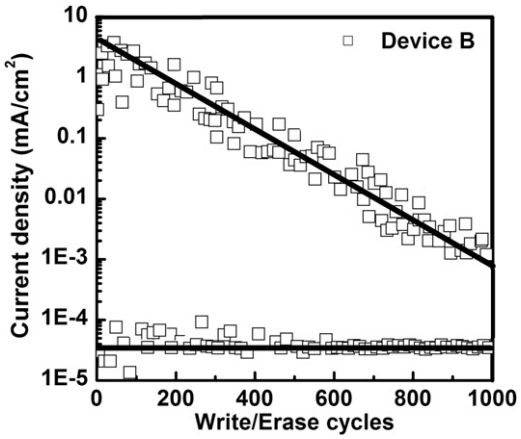

Figure 9. 1000 cycles on–off test results of device B. The line is a guide to the eye.

was located in the middle region of the *m*-MTDATA layer, better cycling endurance was exhibited, but the ON/OFF ratio came down. While the Ag film was close to the Al electrode, the ON/OFF ratio and retention time of those devices decreased sharply, and the bistable phenomenon almost disappeared. Our investigation also presents a simple way to optimize the performance of organic memory by adjusting the location of the Ag layer.

Acknowledgments

The authors are grateful to the Ministry of Science and Technology of China (973 program No. 2006CB921602), the Program for New Century Excellent Talents of Ministry of Educations and the Technology Program of Shaanxi Province (No. 2006K04-c25) for financial support. The authors also wish to thank Mr Zhanwu Yu for providing the AFM images.

References

[1] Scott J C and Bozano L D 2007 *Adv. Mater.* **19** 1452
[2] Scott J C 2004 *Science* **304** 62
[3] Ma L P, Liu J and Yang Y 2002 *Appl. Phys. Lett.* **80** 2997
[4] Ma L P, Pyo S, Ouyang J, Xu Q F and Yang Y 2003 *Appl. Phys. Lett.* **82** 1419
[5] Kondo T, Lee S M, Malicki M, Domercq B, Marder S R and Kippelen B 2008 *Adv. Funct. Mater.* **18** 1112
[6] Su Z S, Fung M K, Lee C S, Li W L and Lee S T 2008 *Appl. Phys. Lett.* **93** 083301
[7] Lauters M, McCarthy B, Sarid D and Jabbour G E 2006 *Appl. Phys. Lett.* **89** 013507
[8] Chen J S and Ma D G 2005 *Appl. Phys. Lett.* **87** 023505
[9] Chen J S, Xu L L, Lin J, Geng Y H, Wang L X and Ma D G 2006 *Appl. Phys. Lett.* **89** 083514
[10] Oyamada T, Tanaka H, Matsushige K, Sasabe H and Adachi C 2003 *Appl. Phys. Lett.* **83** 1252
[11] Chu C W, Ouyang J, Tseng H H and Yang Y 2005 *Adv. Mater.* **17** 1440
[12] Ouisse T and Stephan O 2004 *Org. Electron.* **5** 251
[13] Bozano L D, Kean B W, Beinhoff M, Carter K R, Rice P M and Scott J C 2005 *Adv. Funct. Mater* **15** 1933
[14] Bozano L D, Kean B W, Deline V R, Salem J R and Scott J C 2004 *Appl. Phys. Lett.* **84** 607
[15] Probst M and Haight R 1997 *Appl. Phys. Lett.* **70** 1420
[16] Hirose Y, Kahn A, Aristov V, Soukiassian P, Bulovic V and Forrest S R 1996 *Phys. Rev.* B **54** 13748
[17] Law C W, Lau K M, Fung M K, Chan M Y, Wong F L, Lee C S and Lee S T 2006 *Appl. Phys. Lett.* **89** 133511
[18] Yoshida H and Sato N 2007 *Appl. Phys. Lett.* **91** 141915
[19] Lee J H, Yi Y J and Moon D W 2008 *Appl. Phys. Lett.* **93** 153307
[20] Agrawal R, Kumar P and Ghosh S 2008 *IEEE Trans. Electron Devices* **55** 2795